Actin-binding proteins sensitively mediate F-actin bundle stiffness

Mireille M.A.E. Claessens[1*], Mark Bathe[2*], Erwin Frey[2], Andreas R. Bausch[1]
[1]*Lehrstuhl für Biophysik-E22, Technische Universität München, Garching, Germany*
[2]*Arnold Sommerfeld Center for Theoretical Physics and CeNS, Department of Physics, Ludwig-Maximilians-Universität, Munich, Germany*
**contributed equally to the work*

24 April 2006

Filamentous actin (F-actin) bundles form primary structural components of a broad range of cytoskeletal processes including filopodia, sensory hair cell bristles, and microvilli. *In vivo*, F-actin is bundled by multiple actin-binding proteins (ABPs) that enable the cell to tailor bundle dimensions and mechanical properties to suit diverse biological functions including cell motility, phagocytosis, fertilization, and mechanosensation. Despite the importance of F-actin bundle mechanical properties to many cytoskeletal processes, quantitative investigations of their mediation by actin binding proteins (ABPs) remain scarce. We directly measure the bending stiffness of F-actin crosslinked by three ABPs that are ubiquitous in eukaryotes: I-plastin, fascin-1, and α-actinin and observe distinct regimes of bundle bending stiffness that differ by orders of magnitude depending on ABP type, concentration, and bundle size. The reported behaviour is reproduced quantitatively by a molecular-based mechanical model in which ABP shearing competes with F-actin extension/compression. A generic scaling parameter identifying the relevant bundle bending stiffness regimes is presented. Our results shed new light on the potential role of ABPs in associated cellular processes and demonstrate how single molecule properties determine mesoscopic material properties. Moreover, the observed mechanics of fiber bundle bending are completely general, with broad implications not only for cytoskeletal mechanics but also for the rational design of functional materials.

The mechanical requirements of F-actin bundles are intimately connected to the specific biological function that they are designed to fulfill. Bundles integrated into the cytoskeleton are designed principally to reinforce the cell against mechanical deformation, highly dynamic filopodia present at the leading edge of motile cells are needed to exert potentially large protrusive forces against the advancing membrane during phagocytosis or

migration through the dense extracellular space[1-3], while microvilli are passive structural elements that serve primarily to increase the apical surface area of intestinal epithelial cells, thereby enhancing diffusive nutrient transport. In each case, the cell uses specific ABPs to bundle F-actin and carry out its biological function. α-actinin predominates in cytoskeletal bundles and muscle[4], fascin is prevalent in filopodia[5,6], and plastin is predominant in microvilli and stereocilia[7,8]. The disparate mechanical requirements of these cellular processes, together with the broad evolutionary conservation of their predominant ABPs across vertebrate and invertebrate eukaryotes, suggests that a key component of ABP biological function is its ability to differentially mediate F-actin bundle stiffness[9]. A mechanistic understanding of the effects of ABPs on F-actin bundle mechanics might thus be needed to obtain a complete understanding of their physiological role in cells[10-12]. Quantifying the governing mechanical principles of these fundamental cytoskeletal constituents should also prove valuable in the design of biomimetic nanomaterials[13].

F-actin bundles can be characterized mechanically by their intrinsic bending stiffness, κ_B, which is related to their persistence length, l_p, in the same manner as for any polymer, $\kappa_B = l_p k_B T$. Here, l_p is the length scale over which associated thermal fluctuations destroy memory of a direction initially tangent to the bundle backbone and k_BT denotes thermal energy, where k_B is the Boltzmann constant and T is absolute temperature. κ_B is the mechanical property of interest for F-actin bundles because it can be used to calculate, for example, the maximal force that can be exerted by filopodia prior to buckling[2,3,14] or mechanotransduction mechanisms of brush-border microvilli[15] and hair cell stereocilia[16,17].

Two limiting types of F-actin bundle bending with notably different associated κ_B have been reported (Fig. 1)—*decoupled bending*, in which constituent actin filaments bend independently because intervening crosslinks do not resist shear and instead "tilt" freely during bundle bending[18,19] and *fully coupled bending*, in which filaments are rigidly "glued"

together by intervening crosslinks that strongly resist shear, forcing filaments away from the bundle neutral surface and force them to stretch or compress during bending. The former scenario results in a simple linear dependence of κ_B on the number of filaments, *n*, constituting the bundle. This scaling is what one expects when bending a loose stack of paper and has been observed in the sensory hair bundles of the frog sacculus, predominant in the ABP plastin[18]. In contrast, the latter scenario results in a much stronger *quadratic* dependence, $\kappa_B \sim n^2$, identical to the result for a standard homogeneous mechanical beam, as one would expect if the sheets of paper were glued rigidly together to prohibit interlayer shear deformation. This fully coupled regime was measured quantitatively for the crystalline actin bundle found in the acrosomal process of horseshoe crab sperm cells at fully saturated scruin:actin concentrations[20]. Thus, ABP *type* clearly affects the degree of shear coupling between F-actin filaments and consequently κ_B. However, it is not obvious *a priori* what role specific molecular properties such as ABP shear and extensional stiffness, molecular length, and concentration play in mediating the associated bundle bending regime.

To address these questions, we systematically investigate the dependence of κ_B on bundle size and ABP type and concentration using an emulsion droplet system[21]. Briefly, actin is polymerized in the water phase of a water-dodecane emulsion stabilized by phospholipids. In the absence of bundling proteins, this procedure results in isolated emulsion droplets containing entangled F-actin solutions that can be observed directly using fluorescence microscopy (Fig. 2a). Inclusion of ABPs such as fascin, plastin, or α-actinin in the polymerization process results in a single compact F-actin bundle formed into a closed ring (Fig 2b). As demonstrated theoretically by Odijk[22], the amplitude of the transverse thermal fluctuations of the ring backbone is determined at any given temperature solely by κ_B and the radius of the ring, R_r (Fig. 2b and Methods). Thus, systematic variation of droplet

volume and actin-ABP concentrations in the microemulsion system enables for the first time the controlled investigation of the dependence of κ_B on *n* for each ABP considered (Fig. 2).

For each ABP type and concentration examined, κ_B depends strongly on *n* and converges to the expected single filament value of, 7×10^{-26} Nm^2 ($l_p = 17\times10^{-6}$ m at $T = 298$ K)[23] (Fig. 3a–d). Differences in the dependencies of κ_B on *n* for the different ABP types and concentrations, c_{ABP}, are however drastic. The κ_B of *plastin*-crosslinked bundles increases linearly with *n independently* of $c_{plastin}$ (for $c_{plastin}/c_a \le 0.5$) (Fig 3a), whereas the κ_B of *fascin*-crosslinked bundles depends strongly on both *n* and c_{fascin} (Fig. 3b).

The linear scaling exhibited by κ_B for plastin-crosslinked bundles is consistent with the *decoupled* bending scenario in which F-actin filaments contribute equally and independently to κ_B (Fig. 1), even at high $c_{plastin}:c_a$. We postulate that the physical origin of this observation is that plastin is too weak to resist the inter-filament shear deformation associated with decoupled bundle bending, which is consistent with the crosslink tilting observed in plastin-F-actin bundles using EM[19,24]. Additional support for this hypothesis is provided by the dependence of κ_B on *n* and c_{fascin}, which is quantitatively explained by a purely mechanical model of fiber bundle bending that accounts for the interplay between F-actin *filament stretching* and inter-filament *ABP shearing*[25] (Methods).

In this mechanical model, F-actin is treated as a standard Euler–Bernoulli beam that is capable of extension/compression in addition to pure bending[25] (Fig. 1 and Methods). Crosslinking ABPs mechanically couple neighboring filaments during bundle bending by resisting inter-filament shear with *shear stiffness*, $k_{\|}$. ABP-actin binding affinity and c_{ABP} in the droplet determine the mean axial spacing of ABPs in the bundle, δ, via chemical equilibrium, which gives rise to an *overall effective shear stiffness* coupling neighboring filaments, $k_{\|}/\delta$. The single unknown parameter in the model, $k_{\|}$, is an *intrinsic property* of

any ABP that is a result of protein structure and binding geometry. The bending stiffness of fascin-crosslinked F-actin filaments can be fitted uniquely as a function of both *n* and c_{fascin} using $k_{\|} = 1.5 \times 10^{-5}$ N/m (Fig. 2b). The plastin-concentration-independence of κ_B allows only an upper bound of $k_{\|} \leq 0.05 \times 10^{-5}$ N/m to be calculated.

The crossover in κ_B from n^2- to *n*-scaling has its origin in the finite shear stiffness of the crosslinks. The mechanical model predicts that κ_B must eventually crossover from n^2 to *n*-scaling with increasing *n* due to a competition between crosslink shearing and F-actin filament stretching/compression. Indeed, agreement between the model and experimental data for fascin suggests that this crossover is observed at all but the lowest concentration examined, where a *fully coupled* n^2-scaling at low *n* is superseded by linear scaling at higher *n* (Fig. 3b). This crossover originates from the fact that in order to maintain n^2-scaling, each filament that is successively added to the outer shell of the bundle must be extended/compressed proportionately because the axial strain field in a fully coupled bundle varies *linearly* across the cross-section. The linearly increasing energetic cost of adding filaments to the bundle in this manner must therefore eventually outweigh the cost of shearing the crosslinks instead, which is independent of bundle size. At that point, crosslink shearing relieves filament stretching/compression, leading directly to the crossover in κ_B from fully coupled n^2- to *n*-scaling. This regime is *shear-dominated* and intermediate to the *fully coupled* and *decoupled* regimes. The fact that the crossover in κ_B occurs at decreasing *n* with decreasing fascin concentration (Fig. 3b) is consistent with this picture because it is the *effective* shear stiffness, $k_{\|}/\delta$, that denotes the strength of the shear coupling. A scaling analysis that evaluates the energetic costs of shearing and bending suggests that the dimensionless quantity, $\alpha \equiv k_{\|} L_B^2 / \delta k_a$, denotes the relevant bundle bending regime, where $(\alpha \gg n)$, $(\alpha \ll 1)$, and $(1 \ll \alpha \ll n)$ for the fully coupled, decoupled, and shear-dominated

regimes, respectively. L_B is the bundle length and $k_a = 4.4\times10^{-8}\,\mathrm{N}$ is the axial stretching stiffness of F-actin[26]. This scaling result is generally applicable to any crosslinked fiber bundle provided that k_a is substituted with the appropriate stretching stiffness of the constituent fiber.

Increasing the *length* of the crosslinker shifts the crossover in κ_B to lower *n* because the energetic cost associated with filament stretching/compression in fully coupled bending is proportional to the *distance* of the filament to the center of the bundle. This effect is observed for α-actinin (Fig 3c), which has a molecular length that is roughly three times that of fascin. As a result, the crossover occurs at only $n \approx 3$–4 and a relatively large associated shift in κ_B is observed. Fitting the model to the data yields, $k_{\|} = 10^{-5}$ N/m.

Depletion forces induced by small molecules present in the cytosol may also act as *effective* crosslinkers that bundle F-actin, as demonstrated *in vitro* using polyethylene glycol (PEG)[27,28]. To examine the potential role of depletion forces on F-actin bundle stiffness, we also measured κ_B in the presence of PEG (MW 6 kDa, 2 & 4% w/w). Interestingly, κ_B depends *quadratically* on *n* for the entire range of *n* examined (Fig. 3d), indicating that the bundle remains in the *fully coupled* regime for all bundle sizes investigated ($n < 30$). This places a lower bound on PEG's *effective* crosslinking shear stiffness per unit length of, $k_{\|}/\delta \geq 10^{3}$ N/m^2. This value can be compared directly to the ABPs examined assuming, $\delta = 10^{-7}$ m, the typical ABP axial spacing at high ABP concentration, which results in, $k_{\|} \geq 10^{-4}$ N/m. We postulate that this relatively high stiffness has its origin in a tight inter-molecular packing of the helical F-actin filaments that prohibits inter-filament slip. Given that depletion forces induce fully coupled bundle bending, an important functional role of ABPs *in vivo* might actually be to prevent fully coupled bending by acting as inter-filament spacers.

Folded proteins have complex, anisotropic mechanical properties that depend strongly on secondary and tertiary structure, the magnitude of applied deformations, and the length scales probed[29]. In our experiments thermal fluctuations of the bundle backbone result in ABP shear strains on the order of only one percent. Thus, ABPs are deformed on only the Ångstrom-scale and the observed shear stiffness may be expected to be considerably lower than the extensional stiffness probed by single-molecule unfolding experiments (10^{-3} – 10^{0} N/m) typically with nanometer-resolution[30,31]. The hierarchical structure of proteins allows for a nonlinear mechanical response: a soft response at small deformations is possible without compromising protein stability. Detailed molecular simulations are required to elucidate the precise origin of the observed ABP shear stiffness.

Living cells employ a limited number of ABPs to tightly crosslink F-actin filaments into bundles, and a single ABP type can predominate a given cytoskeletal process. The values of ABP shear stiffness observed here can be used together with the known lengths of physiological bundles to determine the dimensionless parameter, α, and thus the associated bending regime for F-actin bundles found in nature. The *decoupled* bending regime clearly indicates a mechanical preference for maximal bundle compliance, the *fully coupled* regime for maximal bundle stiffness, whereas the *shear-dominated* regime could indicate a preference for an actively tunable bundle stiffness that may be varied between the two limits by varying ABP concentration or bundle size. For example, brush border microvilli are predominant in plastin, range from 2–5 μm in length, and consist of 20–30 filaments. Thus they are in the decoupled bending regime, which could have important biological consequences. Interestingly, due to the typically observed lengths of filopodia, even their bending response is expected to be in this regime. However, it is re-emphasized that we only explore the linear, small deformation shear response of ABPs in this work and nonlinear ABP shear response may be important. A biological advantage of the observed soft shear stiffness of ABPs could be that distinct mechanical response regimes can be fully exploited depending

on the magnitude of bundle deformations. The hierarchical stiffness of proteins and their highly nonlinear response provides an additional means of tuning the bending stiffness of F-actin bundles. It remains a formidable challenge to explore the nonlinear mechanical response of such bundle structures.

Finally, the results presented here highlight the importance of using *in vitro* systems to determine the biomechanical function of ABPs especially considering practical difficulties associated with *in vivo* experiments. Comparing the mechanical properties of bundles formed using a range of ABPs, we demonstrate that bundle mechanics are defined by single molecule properties. It is the formidable challenge of understanding the relation between single molecule structure, mechanics, and the collective behavior of their macromolecular assemblies that is necessary to bridge the existing gap in our understanding of biologically-important processes[10-12]. The governing principles of bundle-bending elucidated in this investigation are completely general and equally applicable to fiber bundles of microtubules or carbon nanotubes as they are to bundles of F-actin. We isolated the dimensionless bundle bending stiffness parameter, α, which may be used in the future to rationally design biological and biomimetic (nano-)materials that employ fiber bundles for enhanced structural stiffness, by tuning the associated bundle bending regime and hence the associated bending stiffness by orders of magnitude.

Methods

Protein preparation. α-actinin is isolated from turkey gizzard smooth muscle[32], dialyzed against G-buffer (2 mM Tris, 0.2 mM ATP, 0.2 mM $CaCl_2$, 0.2 mM DTT, 0.005% NaN_3) and stored at 4 °C for several weeks. Recombinant plasmids containing either the full length human I-plastin cDNa (kind gift from F. Rivero, Köln, Germany) or human fascin (kind gift of D. Vignjevic, Paris, France) are transformed in *Escherichia coli* L12-codon+ bacteria. *E. coli* bacteria carrying the plasmid are grown at 37°C until the A_{600} reached 0.6. Protein expression is induced with isopropyl-β-D-thiogalactopyranoside (IPTG) at 37 °C for I-plastin and at 20°C for fascin. G-actin is extracted from rabbit skeletal muscle according to[33]. G-actin solutions are prepared by dissolving lyophilized G-actin in deionized water and dialyzing against fresh G-buffer at 4ºC for 24 hours. Solutions of G-actin are kept at 4ºC and used within 7 days after preparation. G-actin is polymerized in the presence of ABP and phalloidin TRITC (Sigma)(1:4) inside the water phase of a water-in-dodecane emulsion[21]. Actin polymerization is initiated by adding 1/10th of the sample volume of a 10-fold concentrated F-buffer (20 mM Tris, 20 mM $MgCl_2$, 2 mM $CaCl_2$, 2 mM DTT, and 1 M KCl). After gentle mixing, 20 µl of this solution is immediately transferred to 1 ml of a 0.3 mM phospholipid-containing (95 mol % DOPG, 5 mol % DMPE-PEG2000 (Avanti Polar Lipids)) dodecane solution. Emulsion droplets are subsequently prepared by vortexing the solution for a short time. The negatively charged phospholipids stabilize the droplets against coagulation and mimic the presence of a fluid membrane with essentially no bending undulations. The addition of DMPE-PEG2000 prevented adsorption of filaments and ABPs to the droplet wall. Recombinant I-plastin is reported to bundle actin filaments in the absence, and not in the presence, of calcium. Accordingly, calcium-free actin preparation and F-buffer are used for I-plastin experiments.

Instruments and processing. All data are acquired on a Zeiss Axiovert 200 inverted microscope with a 100x/1.3 NA oil objective. Images are captured at a frame rate of one image per 117 milliseconds with a CCD camera (C4880-80, Hamamatsu) and stored on hard disk. Image storage and analysis are performed with the image processing software "OpenBox"[34]. Samples are maintained in a fluid chamber. Silanization of the glass surface with dichlorodimethylsilane (Sigma) prevented adsorption of the emulsion droplets. To measure the "fuzzy diameter," D_B, of an F-actin bundle in a ring geometry, the fluorescence intensity profile along a line perpendicular to the bundle is followed in time. Fluctuations are followed for 5–12 seconds and the intensity profiles are summed, the width of the distribution is independent of the sampling time, indicating full equilibration. The wall of the droplet merely fixes the center of mass of the ring and does not affect the transverse fluctuations of the bundle. In-plane and out-of-plane transverse fluctuations are equal, confirming that the bundle bending stiffness is isotropic (see Theory). Gaussian distributions are fit to both the instantaneous and the time-averaged fluorescence intensity profiles of the bundle and the standard deviations, σ_{int} and σ_{avg}, respectively, of the distributions are determined. The *fuzzy diameter* of the bundle is, $D_B = \sigma_{avg} - \sigma_{int}$, because σ_{int} does not contribute to the fluctuation amplitude of the bundle. Bundle length L_B was directly proportional to *n* and the experimentally determined linear relation was used in the further analysis.

Theory. A F-actin bundle is assumed to behave like a worm-like chain (WLC) with bending stiffness, κ_B, and contour length L_B. The bending stiffness of a WLC bent into a ring geometry is related to the root-mean-square ring radius, R_c, by[22], $\kappa_B = 0.16 R_c^3 k_B T / D_B^2$, where k_B is the Boltzmann constant, and *T* is absolute temperature. Metropolis Monte Carlo simulations were used to determine the prefactor (0.16) and to confirm that WLCs with transversely isotropic bending stiffness have equal transverse fluctuations in- and out-of-the-plane of the ring. D_B in- and out-of-the-plane of the ring are experimentally determined to be

equivalent, thereby confirming that the bundle bending stiffness is transversely isotropic. To determine the shear stiffness of the crosslinks, κ_B is calculated theoretically using a fiber-based bundle model[25] (MB, EF in preparation 2006). The maximal deflection, $w_{B,max}$, of a bundle subject to a unit load in three-point bending with pinned boundary conditions is calculated analytically using an analogous version of Eq. 11 of ref. 25 and equated with the equivalent displacement of a homogeneous Euler–Bernoulli beam, $\kappa_B = L_B^3 / 48 w_{B,max}$, where,

$$w_{B,max} = \frac{L_B^3}{48 n \kappa_a} - \frac{k_{\|} d (d+t) \sum_{i=1}^{N} i^2}{\delta K n^2 \kappa_a^2} \left[\frac{L_B^3}{24 \beta^2} - \frac{L_B}{2 \beta^4} + \frac{\tanh \frac{\beta L_B}{2}}{\beta^5} \right]$$

$$\beta^2 \equiv \left[\frac{k_{\|}}{\delta K k_a} + \frac{2 k_{\|} d (d+t) \sum_{i=1}^{N} i^2}{\delta K n \kappa_a} \right]$$

and $K \doteq \frac{1}{N} \sum_{k=1}^{N} \sum_{i=k}^{N} i$, where n is the total (odd) number of filaments in 2D and $N \doteq (n-1)/2$. F-actin fibers have stretching stiffness, $k_a = EA = 4.4 \times 10^{-8}$ N[26], and bending stiffness, $\kappa_a = EI = 7.3 \times 10^{-26}$ Nm^2 [35], with diameter $d = 4.5$ nm corresponding to an effective Young's modulus of 2 GPa. The total number of fibers in this 2D theory is related to the number of fibers in 3D, by, $n_{3D} = n_{2D}^2$, and the corresponding 3D bundle bending stiffness is related to the 2D bundle bending stiffness by, $\kappa_{B(3D)} = n_{(2D)} \kappa_{B(2D)}$. δ is the axial spacing between crosslinks and t is the inter-filament spacing, taken to be 10 and 35 nm for fascin/plastin and α–actinin, respectively[24,36,37]. δ is calculated from ABP-actin chemical equilibrium using, $\delta = 33 \times 10^{-9} / \theta$ m, where, $\theta = c_{ABP} / (K_d + c_{ABP})$, is the fraction of bound crosslink sites, K_d is the equilibrium dissociation constant for the relevant ABP binding to F-actin bundles (α–actinin and plastin $K_d = 0.5$ μM, fascin $K_d = 0.7$ μM), and c_{ABP} is the droplet ABP concentration, which is confirmed to be independent of finite-size effects. The minimum mean axial spacing between crosslinks, $\delta_{max} = 33$ nm, corresponds to hexagonally packed F-

actin bundles with fully saturated binding sites. The only unknown parameter in the model, $k_{\|}$, is used to fit the experimental κ_B data uniquely for each ABP crosslink examined.

Acknowledgments

We thank M. Rusp for the actin preparation and M. Schlierf for his help with the protein expression and purification. F. Rivero and D. Vignjevic are acknowledged for the kind gift of recombinant I-plastin and fascin plasmids, respectively. The authors are grateful for useful discussions with C. Heussinger and M. Rief. This work was supported by the DFG (SFB-413) and the Fonds der Chemischen Industrie.

Competing interests. The authors declare that they have no competing interests.

References

1. Borisy, G. G. & Svitkina, T. M. Actin machinery: pushing the envelope. *Curr. Opin. Cell Biol.* **12**, 104-112 (2000).
2. Mogilner, A. & Rubinstein, B. The physics of filopodial protrusion. *Biophys. J.* **89**, 782-795 (2005).
3. Atilgan, E., Wirtz, D. & Sun, X. S. Mechanics and Dynamics of Actin-Driven Thin Membrane Protrusions. *Biophys. J.* **90**, 65-76 (2006).
4. Sanger, J. W., Sanger, J. M. & Jockusch, B. M. Differences in the Stress Fibers between Fibroblasts and Epithelial-Cells. *J. Cell Biol.* **96**, 961-969 (1983).
5. Adams, J. C. Roles of fascin in cell adhesion and motility. *Curr. Opin. Cell Biol.* **16**, 590-596 (2004).
6. Bartles, J. R. Parallel actin bundles and their multiple actin-bundling proteins. *Curr. Opin. Cell Biol.* **12**, 72-78 (2000).
7. Tilney, M. S. et al. Preliminary Biochemical-Characterization of the Stereocilia and Cuticular Plate of Hair-Cells of the Chick Cochlea. *J. Cell Biol.* **109**, 1711-1723 (1989).
8. Lin, C. S., Shen, W. Y., Chen, Z. P., Tu, Y. H. & Matsudaira, P. Identification of I-Plastin, a Human Fimbrin Isoform Expressed in Intestine and Kidney. *Mol. Cell. Biol.* **14**, 2457-2467 (1994).
9. Kureishy, N., Sapountzi, V., Prag, S., Anilkumar, N. & Adams, J. C. Fascins, and their roles in cell structure and function. *BioEssays* **24**, 350-361 (2002).
10. Bausch, A. R. & Kroy, K. A bottom-up approach to cell mechanics. *Nature Phys.* **2**, 231-238 (2006).
11. Gardel, M. L. et al. Elastic Behavior of cross-linked and bundled actin networks. *Science* **304**, 1301-1305 (2004).
12. Storm, C., Pastore, J. J., MacKintosh, F. C., Lubensky, T. C. & Janmey, P. A. Nonlinear elasticity in biological gels. *Nature* **435**, 191-194 (2005).
13. Kis, A. et al. Reinforcement of single-walled carbon nanotube bundles by intertube bridging. *Nature Mat.* **3**, 153-157 (2004).
14. Kovar, D. R. & Pollard, T. D. Insertional assembly of actin filament barbed ends in association with formins produces piconewton forces. *Proc. Natl. Acad. Sci. USA* **101**, 14725-14730 (2004).
15. Do, Z. P. et al. Mechanosensory function of microvilli of the kidney proximal tubule. *Proc. Natl. Acad. Sci. USA* **101**, 13068-13073 (2004).
16. Hudspeth, A. J. & Jacobs, R. Stereocilia Mediate Transduction in Vertebrate Hair-Cells. *Proc. Natl. Acad. Sci. USA* **76**, 1506-1509 (1979).
17. Cotton, J. & Grant, W. Computational models of hair cell bundle mechanics: II. Simplified bundle models. *Hear. Res.* **197**, 105-111 (2004).
18. Howard, J. & Ashmore, J. F. Stiffness of Sensory Hair Bundles in the Sacculus of the Frog. *Hear. Res.* **23**, 93-104 (1986).
19. Tilney, L. G., Egelman, E. H., Derosier, D. J. & Saunders, J. C. Actin-Filaments, Stereocilia, and Hair-Cells of the Bird Cochlea II. Packing of Actin-Filaments in the Stereocilia and in the Cuticular Plate and What Happens to the Organization When the Stereocilia Are Bent. *J. Cell Biol.* **96**, 822-834 (1983).
20. Shin, J. H., Mahadevan, L., So, P. T. & Matsudaira, P. Bending stiffness of a crystalline actin bundle. *J. Mol. Biol.* **337**, 255-261 (2004).
21. Claessens, M. M. A. E., Tharmann, R., Kroy, K. & Bausch, A. R. Microstructure and viscoelasticity of confined semiflexible polymer networks. *Nature Phys.* **2**, 186-189 (2006).

22. Odijk, T. DNA in a liquid-crystalline environment: Tight bends, rings, supercoils. *J. Chem. Phys.* **105**, 1270-1286 (1996).
23. Le Goff, L., Hallatschek, O., Frey, E. & Amblard, F. Tracer studies on F-actin fluctuations. *Phys. Rev. Lett.* **89**, 258101 (2002).
24. Volkmann, N., DeRosier, D., Matsudaira, P. & Hanein, D. An atomic model of actin filaments cross-linked by fimbrin and its implications for bundle assembly and function. *J. Cell Biol.* **153**, 947-956 (2001).
25. Tolomeo, J. A. & Holley, M. C. Mechanics of microtubule bundles in pillar cells from the inner ear. *Biophys. J.* **73**, 2241-2247 (1997).
26. Kojima, H., Ishijima, A. & Yanagida, T. Direct Measurement of Stiffness of Single Actin-Filaments with and without Tropomyosin by in-Vitro Nanomanipulation. *Proc. Natl. Acad. Sci. USA* **91**, 12962-12966 (1994).
27. Hosek, M. & Tang, J. X. Polymer-induced bundling of F actin and the depletion force. *Phys. Rev. E* **69**, 051907 (2004).
28. Tharmann, R., Claessens, M. M. A. E. & Bausch, A. R. Micro- and macrorheological properties of actin networks effectively crosslinked by depletion forces. *Biophys. J.* **90**, 2622-2627 (2006).
29. Li, H. B. et al. Reverse engineering of the giant muscle protein titin. *Nature* **418**, 998-1002 (2002).
30. Schlierf, M. & Rief, M. Temperature softening of a protein in single-molecule experiments. *J. Mol. Biol.* 354, 497-503 (2005).
31. Dietz, H. & Rief, M. Protein structure by mechanical triangulation. Proc. Natl. Acad. Sci. USA 103, 1244-1247 (2006).
32. Craig, S. W., Lancashire, C. L. & Cooper, J. A. Preparation of Smooth-Muscle Alpha-Actinin. Methods Enzymol. 85, 316-321 (1982).
33. Spudich, J. A. & Watt, S. Regulation of Rabbit Skeletal Muscle Contraction .1. Biochemical Studies of Interaction of Tropomyosin-Troponin Complex with Actin and Proteolytic Fragments of Myosin. J. Biol. Chem. 246, 4866-71 (1971).
34. Schilling, J., Sackmann, E. & Bausch, A. R. Digital imaging processing for biophysical applications. Rev. Sci. Inst. 75, 2822-2827 (2004).
35. Gittes, F., Mickey, B., Nettleton, J. & Howard, J. Flexural Rigidity of Microtubules and Actin-Filaments Measured from Thermal Fluctuations in Shape. J. Cell Biol. 120, 923-934 (1993).
36. Edwards, R. A. & Bryan, J. Fascins, a Family of Actin Bundling Proteins. Cell Motil. Cytoskeleton 32, 1-9 (1995).
37. Tang, J. H., Taylor, D. W. & Taylor, K. A. The three-dimensional structure of alpha-actinin obtained by cryoelectron microscopy suggests a model for Ca2+-dependent actin binding. J. Mol. Biol. 310, 845-858 (2001).

Figure captions

Figure 1
F-actin bundle model. F-actin filaments (*black*) are coupled to nearest-neighbor filaments by discrete ABPs (*green*) with axial spacing, δ [m], and shear stiffness, $k_{\|}$ [N/m]. F-actin is characterized mechanically by its backbone extensional stiffness, $k_a = EA = 4.4\times10^{-8}$ N [26], and bending stiffness, $\kappa_B = EI = 7.3\times10^{-26}$ Nm^2 [35], where E is the effective Young's modulus, A is the effective cross-sectional area, and I is the second moment of the cross-sectional area of F-actin. The inter-filament spacing, t, is fixed by the length of the intervening ABPs and remains constant in tightly crosslinked bundles. The ratio, $\alpha \doteq k_{\|}L_B^2/\delta k_a$, where L_B is the bundle length, mediates a competition between crosslink shearing and F-actin filament extension or compression during bundle bending, which determines the bundle bending regime (see text for details).

Figure 2
Experimental setup. a, Isolated F-actin filaments polymerized in an emulsion droplet in the absence of ABPs form a random isotropic solution. **b**, Inclusion of ABPs in the polymerization process leads to the formation of a single F-actin bundle that organizes into a ring of root-mean-square radius, R_r. Actin concentration, c_a, and droplet volume, $V_d = 4\pi R_d^3/3$, where R_d is the droplet radius, determine the total length of F-actin present in the droplet and thus the number of filaments, n, constituting the bundle. Thermal fluctuations of the bundle backbone are characterized by the fuzzy diameter, D, which is directly related to κ_B (Methods). Scale bars are 10 μm.

Figure 3
F-actin bundle bending stiffness, κ_B. a, Bundles crosslinked by plastin exhibit linear scaling in the number of filaments, n, constituting the bundle for both low (○ 1:50) and high (● 1:2) crosslinker:actin concentration ratios, $r_{ABP:a}$. **b,** κ_B for fascin-crosslinked bundles depends strongly on fascin concentration, c_{fascin}, in addition to bundle size ($r_{ABP:a}$ ● 1:2, ○ 1:10, ■ 1:20, □ 1:50). Deviations of the model from experiment at small bundle sizes ($n \le 6$) are attributed to the disordered bundle structure likely present in that regime, which is not accounted for theoretically. **c,** The molecular length of α-actinin is considerably longer than that of fascin or plastin (35 nm versus 10 nm) but has a shear stiffness similar to that of fascin (see text), $r_{ABP:a}$ ● 1:10, ○ 1:50. **d,** F-actin filaments bundled nonspecifically by PEG-induced depletion forces (4% PEG6k ●, 2%PEG6k ○) exhibit a κ_B that increases quadratically in n to large bundle sizes (n ~ 30), yielding a lower bound on the effective crosslinker stiffness per unit length of, $k_{\|}/\delta \ge 10^3$ N/m^2. Dashed lines indicate *decoupled* ($\alpha \ll 1; \kappa_B = n\kappa_a$) and *fully coupled* ($\alpha \gg n; \kappa_B = n^2\kappa_a$) bundle bending regimes assuming zero inter-filament spacing ($t = 0$).

Figures

Figure 1

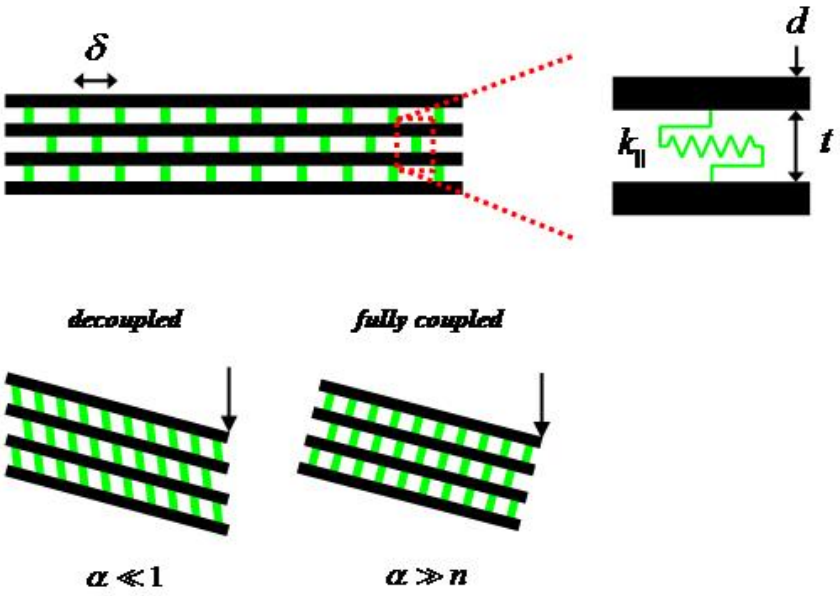

Figure 2

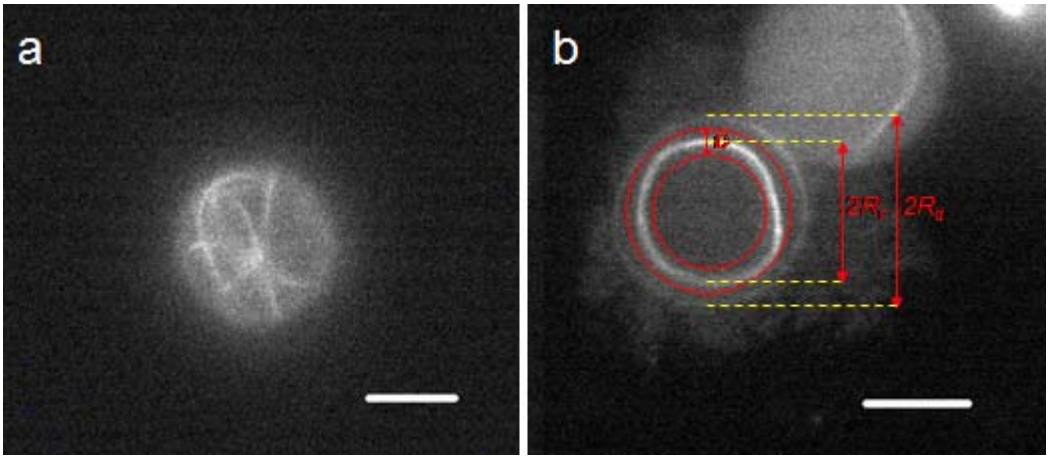

Figure3